IET Microwaves, Antennas & Propagation

Research Article

IET Journals
The Institution of Engineering and Technology

Analysis and synthesis of supershaped dielectric lens antennas

ISSN 1751-8725
Received on 3rd February 2015
Revised on 7th May 2015
Accepted on 27th May 2015
doi: 10.1049/iet-map.2015.0091
www.ietdl.org

Pietro Bia[1], Diego Caratelli[2], Luciano Mescia[1] ✉, Johan Gielis[3]

[1]*Dipartimento di Ingegneria Elettrica e dell'Informazione, Politecnico di Bari, Via E. Orabona 4, 70125, Bari, Italy*
[2]*The Antenna Company Nederland B.V., HighTech Campus, Eindhoven, The Netherlands*
[3]*Department of Bioengineering, University of Antwerp, Groenenborgerlaan 171, 2020 Antwerp, Belgium*
✉ *E-mail: luciano.mescia@poliba.it*

Abstract: A novel class of supershaped dielectric lens antennas, whose geometry is described by the three-dimensional (3D) Gielis' formula, is introduced and analysed. To this end, a hybrid modelling approach based on geometrical and physical optics is adopted in order to efficiently analyse the multiple wave reflections occurring within the lens and to evaluate the relevant impact on the radiation properties of the antenna under analysis. The developed modelling procedure has been validated by comparison with numerical results already reported in the literature and, afterwards, applied to the electromagnetic characterisation of Gielis' dielectric lens antennas with shaped radiation pattern. Furthermore, a dedicated optimisation algorithm based on quantum particle swarm optimisation has been developed for the synthesis of 3D supershaped lens antennas with single feed, as well as with beamforming capabilities.

1 Introduction

Dielectric lens antennas are widely used in various applications, such as radar [1], millimetre wave imaging [2], radio-astronomy [3], as well as broadband wireless communications at high frequencies [4]. The attractive features of this class of antennas primarily consist in the beam collimating/shaping capability, combined with both mechanical and thermal stability, that eases the integration in densely populated electronic circuits.

In the literature, a great deal of attention has been devoted to dielectric lens antennas with canonical (elliptical, spherical, or hyperbolic) and rotationally symmetric shapes [5, 6], optimised in order to enhance the directivity of the antenna and eventually the Gaussicity of the radiated beam [7]. Shaped lenses have been an important topic in several research groups [8, 9], but the effect of multiple internal wave reflections has been investigated only in lens antennas with classical and rotationally symmetric shapes [10–13].

The goal of this research is to present a detailed study of a new class of supershaped dielectric lens antennas whose geometry is described by the so-called Gielis' formula [14, 15]. This formula, which generalises the polar equation of the ellipse, allows the modelling of an extremely wide range of natural objects (plants, stems, starfish, shells, flowers, and more) alongside man-made structures, in a simple and analytical way adjusting a reduced number of parameters. This, in turn, translates into the possibility to automatically reshape the lens profile so that any automated optimisation procedure could be conveniently adopted to identify the geometrical parameters yielding optimal antenna performance.

In the presented contribution, the radiation properties of the mentioned antennas are investigated by means of a dedicated high-frequency technique based on optical ray approximation [16]. In particular, geometrical optics (GO) is adopted to analyse the electromagnetic field propagation within the lens region. In doing so, the contribution of the multiple internal reflections is properly taken into account, so enhancing the accuracy of the modelling procedure, especially when dielectric materials with relatively large permittivity are considered in the design. In this case, the common hypothesis that the energy content relevant to higher order reflected rays can be neglected is not applicable. Finally, by virtue of the equivalence principle and in accordance with the physical optics (PO) approach [16, 17], the far field outside the lens can be evaluated by radiation in free space of the equivalent electric and magnetic current densities on the lens surface. In the developed methodology, these currents are calculated by applying the local Fresnel transmission coefficients along the lens surface to the electromagnetic field evaluated using GO approach. A quantum-inspired version of the particle swarm optimisation (PSO) algorithm, namely the enhanced weighted quantum PSO (EWQPSO) has been specifically developed to perform the design of the supershaped lens antennas yielding optimal antenna performance. Contrary to genetic algorithms (GAs) and other heuristic techniques, the PSO technique does not rely on complicated evolutionary operators, is characterised by reduced computational burden and complexity, allows a more efficient global and local exploration of the search space [18]. In combination with the mentioned asymptotic modelling technique, the EWQPSO procedure allows the recovering, in a time-effective way and with reduced computational cost, of the optimal Gielis' parameters characterising the lens shape.

2 Antenna modelling approach

As shown in Fig. 1, the typical antenna structure considered in this study consists of an electrically large dielectric lens placed at the centre of a perfectly conducting metal disk, with radius r_d, acting as a ground plane and, at the same time, as a shield useful to reduce the back-scattered radiation. The lens is illuminated by the far-field pattern generated by a given electromagnetic source, such as open-ended waveguides, horn antennas, or coaxial probes [19].

Under the assumptions of GO theory, the electric field outside the lens region can be conveniently evaluated as

$$\boldsymbol{E}_t = \sum_{m=0}^{m_{\max}} \boldsymbol{E}_t^m \tag{1}$$

where

$$\boldsymbol{E}_t^m = E_{t\|}^m \frac{\left(\hat{\boldsymbol{n}} \times \hat{\boldsymbol{k}}_t^m\right) \times \hat{\boldsymbol{k}}_t^m}{\left\|\left(\hat{\boldsymbol{n}} \times \hat{\boldsymbol{k}}_t^m\right) \times \hat{\boldsymbol{k}}_t^m\right\|} + E_{t\perp}^m \frac{\hat{\boldsymbol{n}} \times \hat{\boldsymbol{k}}_t^m}{\left\|\hat{\boldsymbol{n}} \times \hat{\boldsymbol{k}}_t^m\right\|} \tag{2}$$

is the transmitted electric field contribution pertaining to the mth

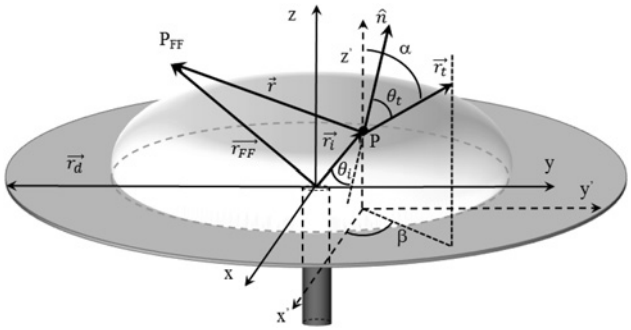

Fig. 1 *Geometry of a dielectric lens antenna. The reference coordinate system used to express the electromagnetic field quantities is also shown*

internal reflection process. In (2), $\hat{\boldsymbol{n}}$ denotes the unit vector normal to the lens surface, $\hat{\boldsymbol{k}}_t^m = \boldsymbol{k}_t^m/||\boldsymbol{k}_t^m||$ is the unit vector of the transmitted wave corresponding to the mth internal reflection with $||\boldsymbol{k}_t^m|| = 2\pi n_0/\lambda_0$, n_0 being the refractive index of the external medium surrounding the lens, λ_0 being the operating wavelength in the vacuum. In particular, $E_{t\|}^m$ and $E_{t\perp}^m$ are the parallel and orthogonal components, respectively, of the transmitted wave contribution due to the mth reflected beam. These field quantities are determined by multiplying the parallel, $E_{i\|}^m$, and orthogonal, $E_{i\perp}^m$, components of the incident electric field, $\boldsymbol{E}_i^m$, on the lens surface with the proper Fresnel transmission coefficients. The evaluation of both $E_{i\|}^m$ and $E_{i\perp}^m$ is carried out using the following equations [8]

$$E_{i\perp}^m = \boldsymbol{E}_i^m \cdot \frac{\boldsymbol{n} \times \hat{\boldsymbol{k}}_i^m}{\left\|\hat{\boldsymbol{n}} \times \hat{\boldsymbol{k}}_i^m\right\|} \tag{3}$$

$$E_{i\|}^m = \boldsymbol{E}_i^m \cdot \frac{\left(\hat{\boldsymbol{n}} \times \hat{\boldsymbol{k}}_i^m\right) \times \hat{\boldsymbol{k}}_i^m}{\left\|\left(\hat{\boldsymbol{n}} \times \hat{\boldsymbol{k}}_i^m\right) \times \hat{\boldsymbol{k}}_i^m\right\|} \tag{4}$$

The incident electric field $\boldsymbol{E}_i^m(P)$ at the point P on the lens surface is directly computed by using the far-field pattern of the source if $m = 1$. On the other hand, for $m > 1$, $\boldsymbol{E}_i^m(P_m)$ is derived starting from the mth reflected wave contribution as

$$\boldsymbol{E}_i^m(P_m) = \boldsymbol{E}_r^{m-1}(P_{m-1})\mathrm{e}^{\mathrm{j}k_i d} \tag{5}$$

where $k_i d$ is the electric length between the observation point P_m and the point P at which the reflection takes place. The reflected field $\boldsymbol{E}_r^{m-1}(P_{m-1})$ appearing in (5) is given by

$$\boldsymbol{E}_r^{m-1}(\mathrm{P}_{m-1}) = E_{r\|}^{m-1}\frac{\left(\hat{\boldsymbol{n}} \times \hat{\boldsymbol{k}}_r^{m-1}\right) \times \hat{\boldsymbol{k}}_r^{m-1}}{\left\|\left(\hat{\boldsymbol{n}} \times \hat{\boldsymbol{k}}_r^{m-1}\right) \times \hat{\boldsymbol{k}}_r^{m-1}\right\|} + E_{r\perp}^{m-1}\frac{\hat{\boldsymbol{n}} \times \hat{\boldsymbol{k}}_r^{m-1}}{\left\|\hat{\boldsymbol{n}} \times \hat{\boldsymbol{k}}_r^{m-1}\right\|} \tag{6}$$

where the parallel, $E_{r\|}^{m-1}$, and orthogonal $E_{r\perp}^{m-1}$ components of the $(m-1)$th reflected wave are computed by multiplying the corresponding components of the $\boldsymbol{E}_i^{m-1}$ with the proper Fresnel reflection coefficients. In (3) and (4), $\hat{\boldsymbol{k}}_i^m = \boldsymbol{k}_i^m/||\boldsymbol{k}_i^m||$ is the unit vector of the incident wave, with $||\boldsymbol{k}_i^m|| = 2\pi n_\mathrm{d}/\lambda_0$, n_d being the refractive index of the dielectric material forming the lens.

Once the GO electromagnetic field has been evaluated, the equivalent electric, $\boldsymbol{J}_\mathrm{s}$, and magnetic, $\boldsymbol{M}_\mathrm{s}$, current densities along the lens surface can be evaluated in a straightforward manner. These current densities, according to the PO formulation, allow the calculation of the electromagnetic far-field radiated by the lens antenna at the observation point $P_{\mathrm{FF}}(r_{\mathrm{FF}}, \theta_{\mathrm{FF}}, \phi_{\mathrm{FF}})$ by considering the integral expression [8]

$$\boldsymbol{E}_{\mathrm{FF}} = \mathrm{j}\frac{\mathrm{e}^{-\mathrm{j}k_0 r_{\mathrm{FF}}}}{2\lambda_0 r_{\mathrm{FF}}}\int_S \left[\eta_0 \boldsymbol{J}_\mathrm{s} \times \hat{\boldsymbol{u}}_0 - \boldsymbol{M}_\mathrm{s}(P)\right] \times \hat{\boldsymbol{u}}_0\, \mathrm{e}^{\mathrm{j}k_0 \boldsymbol{r}\cdot\hat{\boldsymbol{u}}_0}\mathrm{d}S \tag{7}$$

where S is the lens surface, η_0 is the characteristic impedance of the vacuum, r_{FF} is the distance between the observation point P_{FF} and the origin of the coordinate system, $\boldsymbol{r}$ is the vector pointing from the point on the lens P to P_{FF}, and $\hat{\boldsymbol{u}}_0$ is the unit vector corresponding to $\boldsymbol{r}$. In this way, the directivity of the considered radiating system can be obtained by the following expression:

$$h(\theta_{\mathrm{FF}}, \phi_{\mathrm{FF}}) = \frac{4\pi r_{\mathrm{FF}}^2 \left\|\boldsymbol{E}_{\mathrm{FF}}\right\|^2}{\eta_0 P_{\mathrm{tot}}} \tag{8}$$

with P_{tot} being the total power radiated by the lens.

As an alternative to the GO–PO method, a full-GO approach has been, also, developed. In this case, the antenna far field is computed straightforwardly by enforcing the power conservation at the interface of the lens by means of the following formula [8]

$$h\left[\alpha(\theta, \phi), \beta(\theta, \phi)\right] = \frac{K g_t(\theta, \phi)\sin\phi}{\sin\alpha\left[(\partial\alpha/\partial\theta)(\partial\beta/\partial\phi) - (\partial\alpha/\partial\phi)(\partial\beta/\partial\theta)\right]} \tag{9}$$

which provides the intensity of the radiated field in outgoing direction (α, β) from a given point on the lens having spherical coordinates (θ, ϕ). In (9), $g_t(\theta, \phi)$ is the intensity of outgoing transmitted electromagnetic field outside the lens, evaluated as

$$g_t(\theta, \phi) = \left\|\boldsymbol{E}_t\right\|^2 \tag{10}$$

Finally, K is the normalisation constant defined as

$$K = \frac{\text{Far} - \text{field radiated power}}{\text{Lens outgoing power}} = \frac{\int_0^{2\pi}\int_0^{\pi/2} h(\alpha, \beta)\,\mathrm{d}\alpha\,\mathrm{d}\beta}{\int_0^{2\pi}\int_0^{\pi/2} g_t(\theta, \phi)\sin\theta\,\mathrm{d}\theta\,\mathrm{d}\phi} \tag{11}$$

The full-GO method is much faster but less accurate than the combined GO–PO method, and therefore it is just adopted for a preliminary, rough analysis of the considered radiating structure.

In the proposed study, the geometry of the lens is described by the three-dimensional (3D) extension of the so-called superformula, introduced by Gielis, in order to describe complex natural and abstract shapes in a simple and analytical way [14]. In particular, upon assuming a Cartesian coordinate system, the general Gielis' surface can be described in terms of the following parametric equations [20]

$$x = R_\nu R_\mu \cos\nu \cos\mu \tag{12}$$

$$y = R_\nu R_\mu \sin\nu \cos\mu \tag{13}$$

$$z = R_\mu \sin\mu \tag{14}$$

where

$$R_\nu = \left(\left|\frac{\cos(m_1\nu/4)}{a_1}\right|^{n_1} + \left|\frac{\sin(m_2\nu/4)}{a_2}\right|^{n_2}\right)^{-(1/b_1)} \tag{15}$$

$$R_\mu = \left(\left|\frac{\cos(m_3\mu/4)}{a_3}\right|^{n_3} + \left|\frac{\sin(m_4\mu/4)}{a_4}\right|^{n_4}\right)^{-(1/b_2)} \tag{16}$$

In (12)–(16), $\mu \in [0, \pi/2]$ and $\nu \in [-\pi, \pi]$ denote convenient angle parameters. Moreover, $n_p, m_p, b_q \in \mathbb{R}^+$ (positive real numbers), $p = 1, \ldots, 4$ and $q = 1, 2$ and $a_p \in \mathbb{R}_0^+$ (strictly positive real numbers) are selected in such a way that the surface of the lens is closed and characterised, at any point, by curvature radius larger than the working wavelength, in accordance with the GO formulation. The conventional spherical angles θ and ϕ (see

IET Microw. Antennas Propag., 2015, Vol. 9, Iss. 14, pp. 1497–1504

Fig. 1) are obtained from (12)–(14) as

$$\theta = \cos^{-1}\left(\frac{z}{r}\right) \tag{17}$$

$$\phi = \tan^{-1}\left(\frac{y}{x}\right) \tag{18}$$

where $r = \sqrt{x^2 + y^2 + z^2}$.

3 Model validation

The developed GO–PO ray-tracing and tube-tracing procedures have been validated by comparison with the full-wave finite integration technique (FIT) adopted in the commercially available electromagnetic solver CST Microwave Studio. To this end, a supershaped lens antenna with refractive index $n_d = 1.42$ (electric permittivity $\varepsilon_{r_d} = 2.02$), having a maximum radius $r_{max} = 20$ cm and described by the following Gielis' parameters $n_1 = n_2 = n_3 = n_4 = 4$, $a_1 = a_2 = a_3 = a_4 = 1$, $m_1 = m_2 = m_3 = m_4 = 2$, and $b_1 = b_2 = 2$, has been analysed. This radiating structure has been optimised at frequency $f = 10$ GHz. In particular, to reduce the back radiation level, a metal disk with radius $r_p = 40$ cm is used as a ground plane. The antenna feeding is performed using a circular waveguide, having a diameter $a = 4$ cm and filled up with the same dielectric material forming the lens. In addition, to enhance the modelling accuracy, multiple reflection contributions ($m_{max} = 3$) have been taken into account. In Fig. 2, the comparison between the normalised directivity of the antenna as computed by the developed asymptotic techniques and the full-wave analysis based on FIT approach, is shown.

As it can be noticed, a closer agreement with the full-wave results is achieved by using the GO–PO tube-tracing procedure. However, it is important to stress that the rigorous full-wave analysis is by far more demanding in terms of memory occupation and simulation time as the size of the dielectric lens increases. As a matter of fact, using a workstation with dual Intel Xeon E5645 processor, frequency of 2.4 GHz, the computational time and memory allocation required by the full-wave solver are about 17,400 s and 10.3 GByte, respectively. On the other hand, the developed design procedure is characterised by a computational time and memory allocation of 6240 s and 2.5 GByte, on the same workstation. The usefulness of the proposed approach is apparent, especially when antenna synthesis, typically entailing a large number of optimisation steps, is performed. Moreover, in order to highlight the effect of the multiple reflections on the radiation pattern, a more dense dielectric lens, described by the same Gielis' parameters of the previous one, having electric permittivity $\varepsilon_{r_d} = 11.9$ and maximum radius $r_{max} = 10$ cm has been analysed (Fig. 3). The metal disk has radius $r_p = 20$ cm, and the feeding is a circular waveguide having a diameter $a = 3$ cm and filled up with the same dielectric material forming the lens.

4 Synthesis of lens antenna

The Gielis superformula provides the possibility of automatically reshaping the lens profile by acting on a reduced number of parameters. As a result, any automated optimisation procedure can be conveniently adopted in order to identify the lens parameters yielding the optimal antenna characteristic. To this aim, a dedicated novel synthesis procedure based on an improved version of the weighted quantum PSO (WQPSO), has been developed. We refer to the proposed enhanced optimisation method as EWQPSO. Contrary to the conventional PSO algorithm, the considered quantum-inspired version of the PSO permits all particles to have a quantum behaviour instead of the classical Newtonian one. In this way, superior performance in terms of reduced computational times can be achieved, especially when a large number of parameters have to be optimised. Moreover, the EWQPSO is easier to implement since no velocity vectors for particles are

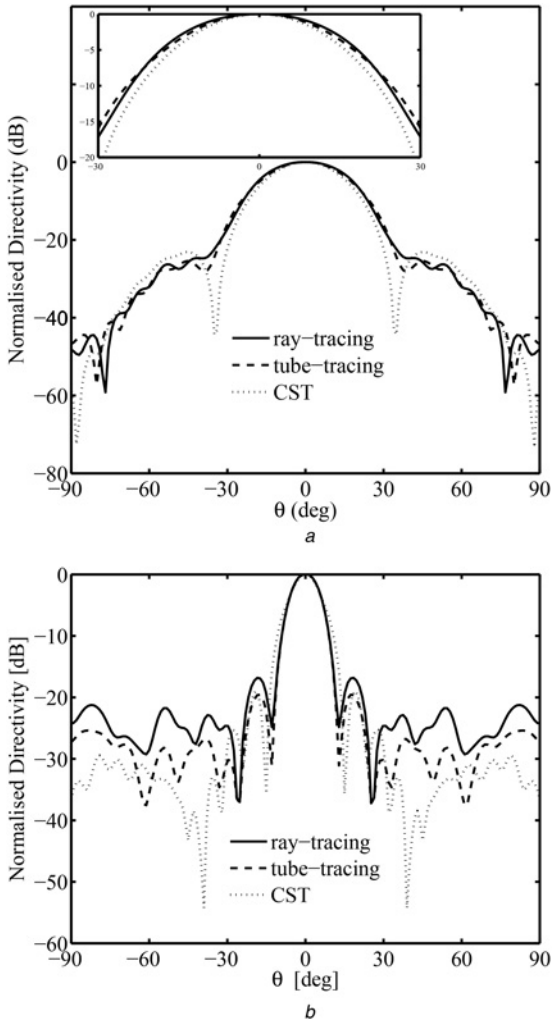

Fig. 2 *Comparison between the normalised directivity of the antenna*

a *H*-plane

b *E*-plane radiation pattern of a supershaped lens as evaluated by GO–PO ray-tracing, GO–PO tube-tracing techniques, and the finite integration technique implemented in the full-wave solver CST Microwave Studio

needed and, therefore, a smaller set of parameters has to be dealt with.

In the conventional WQPSO presented in [21], each particles is located not just in a fixed location, $\boldsymbol{x}_j = [x_{j1}, x_{j2}, \ldots, x_{jN}]^T$, but probabilistically in complete N-dimensional search space according to a probability density function (pdf) obtained by solving the following Schrodinger equation

$$j\hbar \frac{\partial Q(\boldsymbol{r}_j, t)}{\partial t} = \hat{H}(\boldsymbol{r}_j) Q(\boldsymbol{r}_j, t) \tag{19}$$

with $\hbar$ is the Plank constant divided by 2π, and where $\hat{H}(\boldsymbol{r})$ denotes the time-independent Hamiltonian operator that is

$$\hat{H}(\boldsymbol{r}_j) = -\frac{\hbar^2}{2m}\nabla^2 + V(\boldsymbol{r}_j) \tag{20}$$

where m denotes the mass of the particle (in the simulations equal to 1), and $\boldsymbol{r}_j$ is the N-dimensional distance vector between the evaluated position $\boldsymbol{x}_j$ of the jth particle and the position $\boldsymbol{p}_j$ of the local attractor. In (20), $V(\boldsymbol{r}_j)$ is the potential function defined as a Dirac distribution centred in $\boldsymbol{p}_j$. In the following, let us denote the coordinate of the personal best location of the jth particle as $\boldsymbol{x}_{bj}(t)$ and the global best location as $\boldsymbol{x}_g(t)$. Under these assumptions,

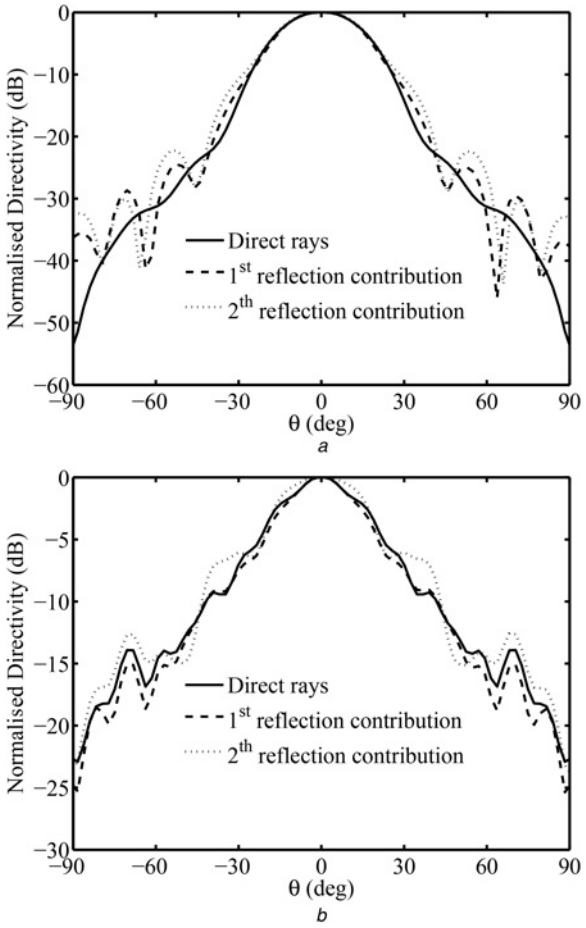

Fig. 3 *Comparison between the normalised directivity of the antenna*

a *H*-plane

b *E*-plane radiation pattern of a supershaped lens as evaluated by GO–PO tube-tracing techniques considering simple direct rays, first and second reflection contributions for a lens having electric permittivity $\varepsilon_{r_d} = 11.9$

each local attractor is positioned in

$$\boldsymbol{p}_j(t) = \varphi_j \boldsymbol{x}_{bj}(t) + (\mathrm{I} - \varphi_j)\boldsymbol{x}_{\mathrm{g}}(t) \tag{21}$$

with $j = 1, \ldots, M$, where M is the number of particles, and where φ_j is a $M \times N$ diagonal matrix having diagonal elements values uniformly distributed in the interval [0, 1]. Upon solving (19), the pdf $Q(\boldsymbol{r}_j)$ and the updated position $\boldsymbol{x}_j(t+1)$ of the general particles are found to be, respectively

$$Q(\boldsymbol{r}_j, t) = \frac{1}{\boldsymbol{L}_j(t)} \exp\left\{-2\frac{|\boldsymbol{r}|}{\boldsymbol{L}_j(t)}\right\} \tag{22}$$

$$\boldsymbol{x}_j(t+1) = \begin{cases} \boldsymbol{p}_j(t) + \dfrac{\boldsymbol{L}_j(t)}{2}\ln\left(\dfrac{1}{\boldsymbol{u}_j}\right) & \text{with } \boldsymbol{\psi}_j > 0 \\ \boldsymbol{p}_j(t) - \dfrac{\boldsymbol{L}_j(t)}{2}\ln\left(\dfrac{1}{\boldsymbol{u}_j}\right) & \text{with } \boldsymbol{\psi}_j \le 0 \end{cases} \tag{23}$$

where $\boldsymbol{\psi}_j$ and $\boldsymbol{u}_j$ are two $N \times 1$ column vectors having elements values uniformly distributed in the interval [0, 1], and $\boldsymbol{L}_j(t)$ is a $N \times 1$ column vector denoting the standard deviation of the pdf of each particle evaluated as

$$\boldsymbol{L}_j(t) = 2\beta|\boldsymbol{m}(t) - \boldsymbol{x}_j(t)| \tag{24}$$

with β being the contraction–expansion coefficient, whose value ranges from 0.5 to 1. Generally, β is a function of the generation index. In the framework of the conventional WQPSO algorithm, the mean best coordinates $\boldsymbol{m}(t)$ are evaluated as follows:

$$\boldsymbol{m}(t) = \frac{1}{M}\sum_{j=1}^{M} \alpha_j \boldsymbol{x}_{bj}(t) \tag{25}$$

where α_j is a suitable weighting coefficient linearly from 1.5, for the best particle, down to 0.5 for the worst one. The developed EWQPSO technique differs from the WQPSO prominently in the definition of $\boldsymbol{m}(t)$. In particular, the following adaptive generation-dependent update equation is used

$$\boldsymbol{m}(t) = \frac{\sum_{j=1}^{M}\left(1 - \left(F(\boldsymbol{x}_{bj})/\left(\max\left[F(\boldsymbol{x}_{b1}), \ldots, F(\boldsymbol{x}_{bM})\right]\right)\right)\right)\boldsymbol{x}_{bj}(t)}{\sum_{j=1}^{M}\left(1 - \left(F(\boldsymbol{x}_{bj})/\left(\max\left[F(\boldsymbol{x}_{b1}), \ldots, F(\boldsymbol{x}_{bM})\right]\right)\right)\right)} \tag{26}$$

Each particle is relevant to a specific parameter affecting the shape and size of the lens antenna, as well as the position of the feed and the refractive index of the material forming the lens. In (26), the fitness function value F is evaluated as

$$F(\boldsymbol{x}_{bj}) = \sum_{l=1}^{N_\theta}\sum_{m=1}^{N_\phi}\left|\frac{\overline{h}_{l,m}^{\mathrm{T}} - \overline{h}_{l,m}^{j}}{1 + \overline{h}_{l,m}^{\mathrm{T}}}\right| \tag{27}$$

where $\overline{h}^{\mathrm{T}}$ is the target normalised directivity, expressed in dB, and $\overline{h}^{j}$ is the normalised directivity, in dB, relevant to the jth particle. In (28), N_θ and N_ϕ denote the number of points in which the azimuthal and polar coordinates are discretised, respectively. The optimisation procedure stops when the fitness value of the global best particle is smaller than a given threshold (which in the current study has been set to 10^{-3}) or, alternatively, when the maximum number of particle generations is reached. The fitness function (27) has been engineered in order to obtain reliable numerical results and a fast convergence of the antenna directivity to the target one.

In order to enhance the effectiveness of the proposed lens synthesis tool, a dynamic selection of the antenna analysis technique is performed. In particular, upon denoting the maximum number of particle generations with $g_{\max}$ and current generation with g, the optimisation algorithm is based on three main steps. During the first step, when $1 \le g \le g_{\max}/6$, the full-GO technique is adopted. This methodology is computationally inexpensive and fast, although less accurate and, therefore, it allows discarding efficiently the worst antenna configurations during the first stages of the PSO procedure. As soon as the number of generations increases ($g_{\max}/6 \le g \le g_{\max}/3$) and the particles tend to get closer to the optimal lens geometry (second step), the GO–PO ray tracing method is used. This technique provides a higher accuracy in the characterisation of the best solution candidates, although it requires larger computational resources and time because of the numerical burden related to the evaluation of the equivalent electric and magnetic current densities. Finally, during the third step, when $g_{\max}/3 \le g \le g_{\max}$, the GO–PO tube tracing method with conformal tessellation of the lens surface is applied in order to achieve a more accurate modelling of multiple internal reflections and, therefore, more rigorous characterisation of the antenna solutions. Of course, the use of the GO–PO methodology results in an extra computational burden. It has to be stressed that the illustrated procedure has been adjusted heuristically by analysing the features of the typical problem space for the synthesis of Gielis' lens antennas. The flowchart relevant to the GO–PO tube tracing algorithm is shown in Fig. 4.

The validation of the developed EWQPSO optimisation tool has been carried out by synthesising a lens antenna featuring a flat-top radiation pattern at frequency $f = 60$ GHz (see Fig. 5). The structure is assumed fed by a rectangular patch having dimensions $a = 1.2$ and $b = 0.9$ mm, working on the fundamental mode, and backed by a circular metal ground plane with radius $r_p = 60$ mm (see Fig. 1). A swarm of $M = 24$ particles has been used for the optimisation procedure carried out over $g_{\max} = 40$ generations. The

IET Microw. Antennas Propag., 2015, Vol. 9, Iss. 14, pp. 1497–1504

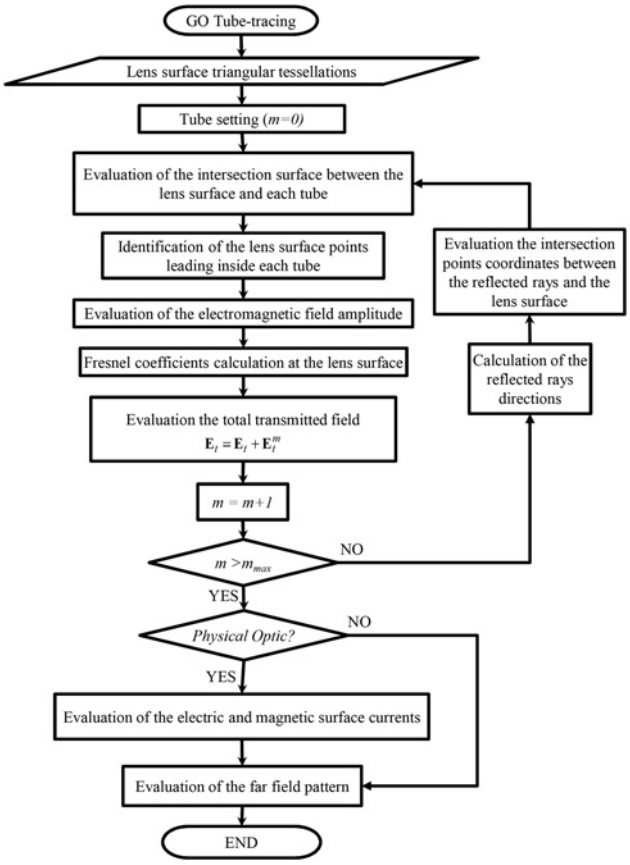

Fig. 4 *Flowchart of the tube-tracing method*

position vector is $\boldsymbol{x} = [n_1, n_2, m_1, m_2, n_3, n_4, m_3, m_4, b_1, b_2, n_d, r_{\min}]^{\mathrm{T}}$. The multidimensional search space has been restricted by assuming that the parameters n_1, n_2, m_1, m_2, n_3, n_4, m_3, m_4, b_1, b_2 can range from 1 to 5, n_{d} can vary between 1.7 ($\varepsilon_{r_{\mathrm{d}}} \simeq 2.9$) and 3 ($\varepsilon_{r_{\mathrm{d}}} \simeq 9$), the minimum lens radius $r_{\min}$ is assumed to range from 20 to 50 mm, whereas the Gielis' parameters a_1, a_2, a_3, a_4 are all set to 1. The location of the feeding patch is $x = y = 0$ (see Fig. 1).

Under these assumptions, by using the EWQPSO procedure, the optimal lens parameters are found to be: $n_1 = 2.480$, $n_2 = 2.297$, $m_1 = 1.503$, $m_2 = 1.609$, $n_3 = 2.986$, $n_4 = 1.779$, $m_3 = 1.948$, $m_4 = 2.845$, $b_1 = 4.638$, $b_2 = 4.888$, $n_d = 1.8$ ($\varepsilon_{r_{\mathrm{d}}} \simeq 3.2$), and $r_{\min} = 27.9$ mm corresponding to $r_{\max} = 29.8$ mm. The resulting lens geometry is shown in Fig. 6. As it appears from Fig. 6, the synthesised radiation patterns are in excellent agreement with the target flat-top masks along both the *E* and *H* planes of the antenna. Moreover, it is clear that accounting for the multiple wave reflections occurring within the lens is instrumental to the enhancement of the modelling accuracy of the procedure.

Fig. 7 shows the convergence rate of the new optimisation procedure (EWQPSO), as well as of the WQPSO, the classical PSO and GA, when applied to the synthesis of the lens antenna illustrated in Fig. 5. In particular, a conventional binary encoded GA with stochastic uniform selection, scattered crossover, and low probability mutation rate has been employed to this end. Clearly, the EWQPSO outperforms both the PSO and GA, as well as the conventional WQPSO in terms of convergence rate, accuracy, and population size. These properties of the EWQPSO are highly attractive in the considered contest where the computational burden associated with the computation of the fitness function is not negligible.

5 Numerical example

The design of a lens antenna with electronic beam-steering capability is detailed in this section. As shown in Fig. 8, the feeding of the

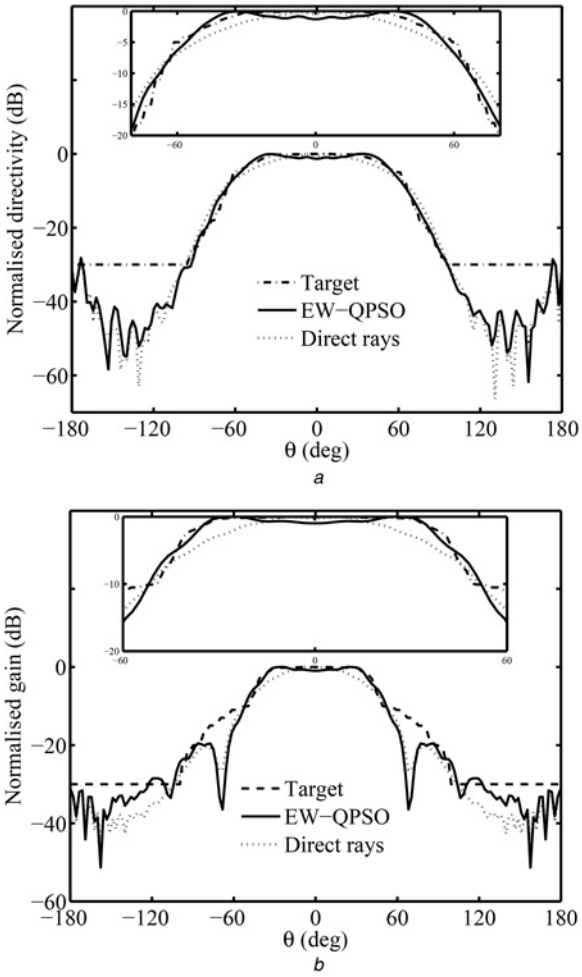

Fig. 5 *Validation of the developed EWQPSO optimisation tool*

a *H*-plane
b *E*-plane radiation pattern of a Gielis' lens antenna synthesised by means of the EWQPSO procedure. The target flat-top mask and simpler direct rays results are also shown

radiating structure is carried out by means of a linear array of five patch antennas optimised in such a way as to achieve good return-loss characteristics in combination with a reasonably small coupling level at the working frequency $f = 60$ GHz. The geometry of the patch array is also illustrated in Fig. 8. The dielectric substrate has a refractive index of 1.8, whereas the antenna element spacing is set to be $\lambda/2$, with λ denoting the working wavelength in the dielectric lens.

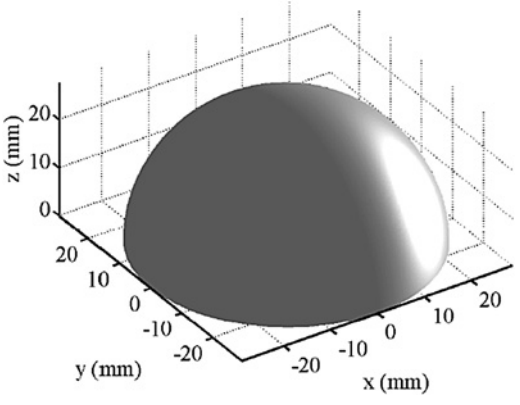

Fig. 6 *Shape of the lens synthesised by means of the EWQPSO procedure in order to ensure a flat-top radiation pattern at 60 GHz*

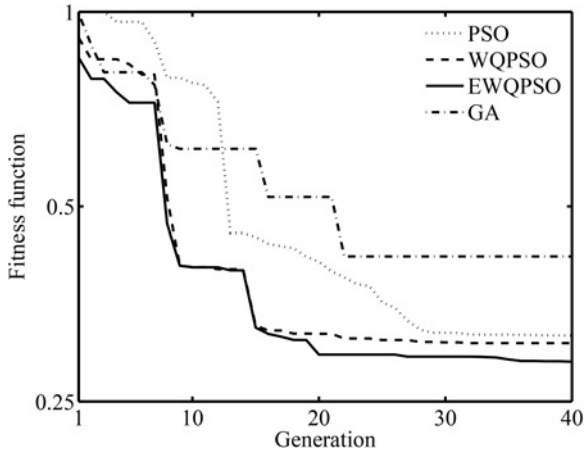

Fig. 7 *Convergence rate of the EWQPSO, WQPSO, classical PSO, and GA when applied to the synthesis of the lens antenna shown in Fig. 6. The same number of iterations and population are adopted for the considered algorithms*

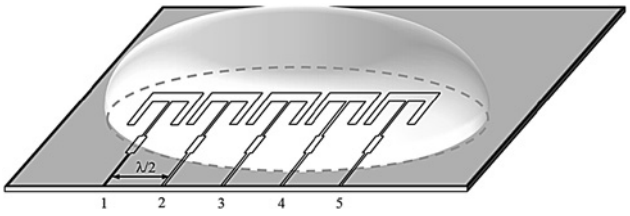

Fig. 8 *Sketch of the linear patch antenna array used as feeding structure of a supershaped antenna for 60 GHz wireless communications*

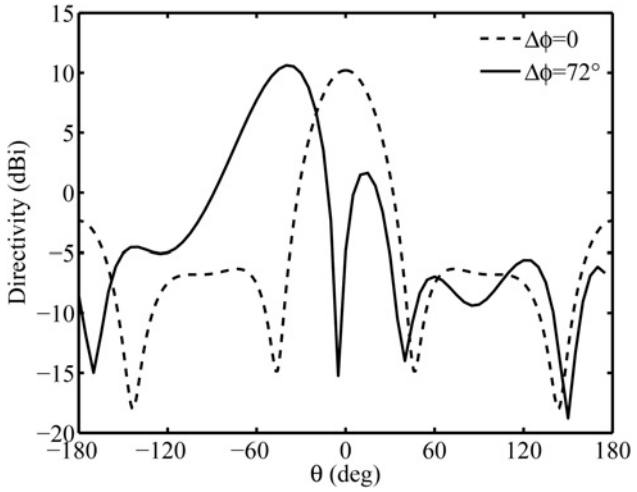

Fig. 9 *Radiation patterns of the patch antenna array without dielectric lens for different beam-steering angles. Working frequency f = 60 GHz*

As shown in Fig. 9, the radiation pattern of the basic array structure can be electronically steered by changing the phase shift $\Delta\phi$ between adjacent patches. It has been found out that the array directivity ranges from 10.7 dBi for $\Delta\phi = 0$ to 11.0 dBi for $\Delta\phi = 72°$ with a side-lobe level (SLL) of −9 dBi at the maximum steering angle of 40°. The antenna performance in term of directivity, steering angle, and SLL can be enhanced by integrating a suitable dielectric lens (see Fig. 7), whose geometry has been optimised by means of the EWQPSO technique presented in Section 4. To this end, a swarm of $M = 24$ particles has been used for the optimisation procedure carried out over $g_{max} = 40$ generations. The search domain has been restricted by assuming

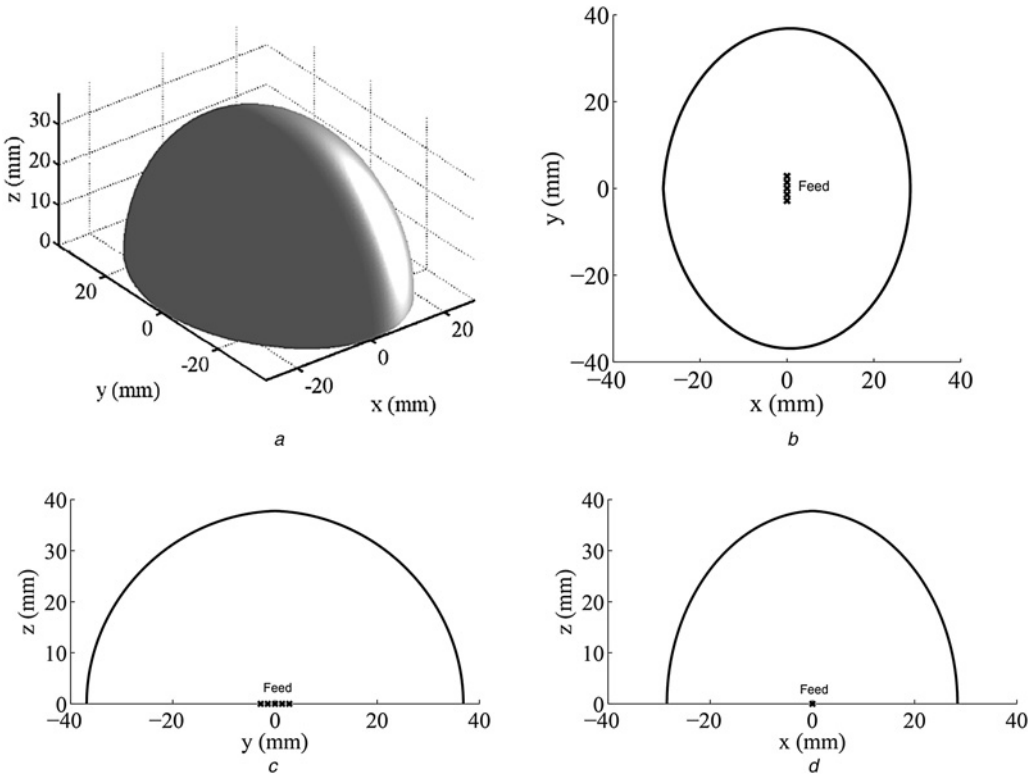

Fig. 10 *Resulting lens geometry*

a Optimal lens shape synthesised for electronic beam steering, at 60 GHz, of the patch antenna array shown in Fig. 8
b $z = 0$ cutting plane
c $x = 0$ cutting plane
d $y = 0$ cutting plane

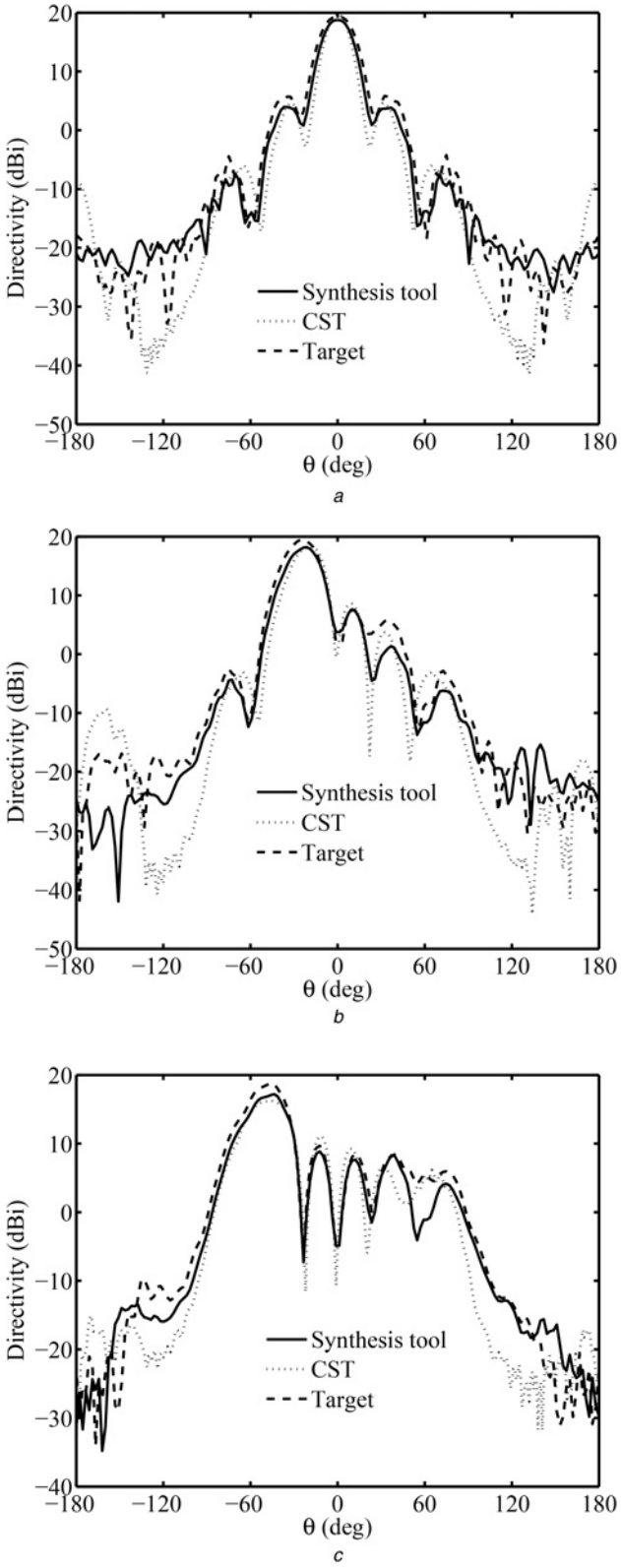

Fig. 11 *H-plane radiation pattern of a lens-integrated patch antenna array for different phase excitations*

a $\Delta\phi = 0°$
b $\Delta\phi = 72°$
c $\Delta\phi = 144°$

that the lens parameters n_1, n_2, m_1, m_2, n_3, n_4, m_3, m_4, b_1, b_2 can range from 1 to 5, whereas the parameters a_1, a_2, a_3, a_4 are all set to 1. Furthermore, the refractive index n_d of the material forming the lens can vary from 1.7 to 3 and, finally, the minimal lens radius r_{min} is assumed to range from 20 to 30 mm.

Under these assumptions, by using the EWQPSO procedure, the optimal lens parameters are found to be: $n_d = 1.76$, $r_{min} = 28.4$ mm, $n_1 = 4.341$, $n_2 = 4.054$, $m_1 = 1.902$, $m_2 = 2.072$, $n_3 = 3.896$, $n_4 = 4.008$, $m_3 = 1.875$, $m_4 = 1.947$, $b_1 = 2.398$, and $b_2 = 2.161$ with the feeding patch array being centred in the origin of the coordinate system. The resulting lens geometry is shown in Fig. 10. The rotational asymmetry of the structure can be noticed. In Fig. 11 the *H*-plane radiation pattern of the array for the excitation phase shifts $\Delta\phi = 0$, $\Delta\phi = 72°$, and $\Delta\phi = 144°$ is shown.

As it can be noticed in Fig. 11, the considered antenna structure is characterised by a SLL of −10 dBi for scanning angles up to 50°. Furthermore, the lens integration allows achieving a larger peak directivity value ranging from 18.3 dBi for $\Delta\phi = 0$ to 17.2 dBi for $\Delta\phi = 144°$. It is important to notice in Fig. 11 the good agreement between the results obtained by applying the proposed design approach and those computed by using the commercial electromagnetic solver CST Microwave Studio.

6 Supershaped lens antenna innovations

In comparison to know classes of shaped lenses, the supershaped dielectric lens antenna technology provides a higher degree of versatility allowing the antenna tailoring and optimisation for a wide variety of applications. In particular, the unified geometrical description provided by the Gielis transformations allows an accurate characterisation in terms of circuital and radiation properties set by a specific lens shape. In fact, the use of (12)–(16) makes possible the analytical evaluation of the lens volume and area, vertex sharpness (or roundness), sides convexity (or concavity), aspect ratio, as well as a preliminary analysis of the antenna performance in terms of matching bandwidths, radiation efficiency, and stability of the radiation patterns. By properly adjusting the numerical parameters in (15)–(16) a virtually infinite variety of shapes can be generated and optimised in order to synthesise complex radiation pattern mask with broad and stable operation over large frequency ranges. Moreover, wide-band performance in terms of input impedance matching, radiation patterns, realised gain, and polarisation properties has been obtained using supershaped antennas [15].

The superformula also provides a number of benefits regarding the modelling approach. In particular, with reference to the GO–PO formulation, the Gielis' transformation allows the analytical calculation of the main physical quantities involved the electromagnetic propagation problem within the lens (see Appendix). In this way, a smaller computational burden, reduced algorithm complexity, and eventually more accurate numerical results can be obtained. In conclusion, the use of the Gielis' formula allows a multifold improvement of lens antenna characteristics while easing the relevant electromagnetic modelling.

7 Conclusion

A novel design procedure for supeshaped dielectric lens antennas has been presented. To this end, a GO–PO formulation is used for modelling the multiple reflection processes occurring within the lens. The proposed model has been validated by comparison with the results obtained using the full-wave electromagnetic solver CST Microwave Studio. In order to synthesise lens antennas featuring a given radiation mask, a dedicated EWQPSO optimisation procedure has been developed. By using the design tool one can retrieve the optimal lens geometry, size, and material characteristics useful to achieve the desired antenna performance. The applicability of the new optimisation procedure was investigated by studying the problem of synthesis of lens antennas having flat-top radiation characteristics as well as electronic beam-steering capability for 60 GHz wireless communications. The performance of the EWQPSO was shown to outperform both the WQPSO and the classical PSO most of the time in the convergence rate as well as in the final error level. The obtained results have been found to be in good agreement with those

computed by full-wave simulations. The proposed design tool could be usefully adopted to design complex Gielis' lens antennas, for a wide variety of applications ranging from microwave imaging to the mm-wave communications, where enhanced directivity, and complex radiation patterns are needed for optimal radio coverage and illumination, improved efficiency, and reduced electromagnetic interferences between devices sharing the same platform.

8 References

1 Uehara, K., Miyashita, K., Natsuma, K., Hatakeyama, K., Mizuno, K.: 'Lens-coupled imaging arrays for the millimeter- and submillimeterwave regions', *IEEE Trans. Microw. Theory Tech.*, 1992, **40**, pp. 806–811

2 Raman, S., Barker, N.S.: 'AW-band dielectric-lens-based integrated monopulse radar receiver', *IEEE Trans. Microw. Theory Tech.*, 1998, **46**, pp. 2308–2316

3 Bttgenbach, T.H.: 'An improved solution for integrated array optics in quasioptical mm and submm receivers: the hybrid antenna', *IEEE Trans. Microw. Theory Tech.*, 1998, **41**, pp. 1750–1761

4 Rolland, A., Sauleau, R., Coq, L.L.: 'Flat-shaped dielectric lens antenna for 60-ghz applications', *IEEE Trans. Antennas Propag.*, 2011, **59**, pp. 4041–4048

5 Filipovic, D.F., Rebeiz, G.M.: 'Double-slot antennas on extended hemispherical and elliptical quartz dielectric lenses', *Int. J. Infrared Millimeter Waves*, 1993, **14**, pp. 1905–1924

6 Lee, J.J.: 'Handbook of microwave and optical components' (K. Chang Ed. Wiley, New York, 1989)

7 Boriskin, A., Boriskina, S., Godi, G., Sauleau, R., Nosich, A.: 'Small hemielliptic dielectric lens antenna analysis: boundary integral equations vs. go and po'. European Microwave Conf., 4–6 October 2005

8 Chantraine-Bars, B., Sauleau, R., Coq, L.L.: 'A new accurate design method for millimeter-wave homogeneous dielectric substrate lens antennas', *IEEE Trans. Antennas Propag.*, 2005, **53**, pp. 1069–1082

9 Dang, T., Yang, J., Zheng, H.: 'An integrated lens antenna design with irregular lens profile'. Fifth Global Symp. on Millimeter Waves, 2012, pp. 212–215

10 Boriskin, A., Godi, G., Sauleau, R., Nosich, A.: 'Small hemielliptic dielectric lens antenna analysis in 2-D: boundary integral equations versus geometrical and physical optics', *IEEE Trans. Antennas Propag.*, 2008, **56**, pp. 485–492

11 Pavacic, A.P., del Ro, D.L., Mosig, J.R., Eleftheriades, G.V.: 'Three-dimensional ray-tracing to model internal reflection in off-axis lens antennas', *IEEE Trans. Antennas Propag.*, 2006, **54**, pp. 604–612

12 Neto, A., Maci, S., de Maagt, P.J.I.: 'Reflections inside an elliptical dielectric lens antenna', *IEE Proc. Microw. Antennas Propag.*, 1998, **145**, pp. 243–247

13 Hailu, D., Ehtezazi, I.A., Safavi-Naeini, S.: 'Fast analysis of terahertz integrated lens antennas employing the spectral domain ray tracing method', *IEEE Antennas Wirel. Propag. Lett.*, 2009, **8**, pp. 37–39

14 Gielis, J.: 'A generic geometric transformation that unifies a wide range of natural and abstract shapes', *Am. J. Botany*, 2003, **90**, pp. 333–338

15 Simeoni, M., Cicchetti, R., Yarovoy, A., Caratelli, D.: 'Plastic-based supershaped dielectric resonator antennas for wide-band applications', *IEEE Trans. Antennas Propag.*, 2011, **59**, pp. 4820–4825

16 Balanis, C.A.: 'Antenna theory: analysis and design' (John Wiley and Sons, Hoboken, 2005, 3rd edn.)

17 Nguyen, N.T., Rolland, A., Sauleau, R.: 'Range of validity and accuracy of the hybrid GO-PO method for the analysis of reduced-size lens antennas: benchmarking with BoR-FDTD'. Asia-Pacific Microwave Conf., 2008, pp. 1–4

18 Fornarelli, G., Mescia, L.: 'Swarm intelligence for electric and electronic engineering' (IGI Global, Hershey PA, 2013)

19 Lo, Y.T., Lee, V.S.W.: 'Antenna handbook' (Van Nostrand Reinhold, New York USA, 1993), vol. 2

20 Bia, P., Caratelli, D., Mescia, L., Gielis, J.: 'Electromagnetic characterization of supershaped lens antennas for high-frequency applications'. Proc. of the 43rd European Microwave Conf., 2013, pp. 1679–1682

21 Xi, M., Sun, J., Xu, W.: 'An improved quantum-behaved particle swarm optimization algorithm with weighted mean best position', *Appl. Math. Comput.*, 2012, **205**, pp. 751–759

9 Appendix

In this appendix, the analytical expressions of physical quantities used in the GO and PO procedures are provided. In particular, taking into account that the unit vector, $\hat{\boldsymbol{t}}$, tangent to the lens surface, the transmitted unit wave vector $\hat{\boldsymbol{k}}_t$, and the reflected unit wave vector $\hat{\boldsymbol{k}}_r$ are given by

$$\hat{\boldsymbol{t}} = -\frac{\hat{\boldsymbol{n}} \times \left(\hat{\boldsymbol{n}} \times \hat{\boldsymbol{k}}_i\right)}{\left\|\hat{\boldsymbol{n}} \times \left(\hat{\boldsymbol{n}} \times \hat{\boldsymbol{k}}_i\right)\right\|} \tag{28}$$

$$\hat{\boldsymbol{k}}_t = \cos\theta_t \hat{\boldsymbol{n}} + \sin\theta_t \hat{\boldsymbol{t}} \tag{29}$$

$$\hat{\boldsymbol{k}}_r \times \hat{\boldsymbol{n}} = \left(\sin\theta_i - \cos\theta_i\right)\hat{\boldsymbol{n}} \tag{30}$$

the propagation problem can be fully solved if the expression defining the unit vector $\hat{\boldsymbol{n}}$ normal to the lens surface is known.

The unit vector $\hat{\boldsymbol{n}}$ is defined as follows:

$$\hat{\boldsymbol{n}} = \frac{(\partial \boldsymbol{r}/\partial\theta)(\partial \boldsymbol{r}/\partial\phi)}{\left\|(\partial \boldsymbol{r}/\partial\theta) \times (\partial \boldsymbol{r}/\partial\phi)\right\|} \tag{31}$$

where the derivatives of the radius vector $\boldsymbol{r}(\theta, \phi)$ are given by

$$\frac{\partial \boldsymbol{r}}{\partial\theta} = \frac{\partial r}{\partial\theta}\hat{\boldsymbol{r}} + r\hat{\boldsymbol{\theta}} \tag{32}$$

$$\frac{\partial \boldsymbol{r}}{\partial\phi} = \frac{\partial r}{\partial\phi}\hat{\boldsymbol{r}} + r\sin\theta\hat{\boldsymbol{\phi}} \tag{33}$$

with

$$\frac{\partial r}{\partial\theta} = \frac{\partial r}{\partial\mu}\frac{\partial\mu}{\partial\theta} \tag{34}$$

$$\frac{\partial r}{\partial\phi} = \frac{\partial r}{\partial\nu} - \tan\gamma\frac{\partial r}{\partial\theta} \tag{35}$$

$$\gamma = \mathrm{a}\tan\left(\frac{\partial\theta}{\partial\mu}\right) \tag{36}$$

Considering the general equation describing the Gielis' surface, the following expression can be obtained

$$\frac{\partial r}{\partial\mu} = \frac{1}{r}\left(x\frac{\partial x}{\partial\mu} + y\frac{\partial y}{\partial\mu} + z\frac{\mathrm{d}z}{\mathrm{d}\mu}\right) \tag{37}$$

$$\frac{\partial\mu}{\partial\theta} = \left[r\frac{(\mathrm{d}z/\mathrm{d}\mu) - z(\partial r/\partial\mu)}{r^2\sqrt{1-\left(z/r\right)^2}}\right]^{-1} \tag{38}$$

where

$$\frac{\partial x}{\partial\mu} = R_\nu\frac{\mathrm{d}R_\mu}{\mathrm{d}\mu}\cos\mu\cos\nu - R_\mu R_\nu\sin\mu\cos\nu \tag{39}$$

$$\frac{\partial y}{\partial\mu} = R_\nu\frac{\mathrm{d}R_\mu}{\mathrm{d}\mu}\cos\mu\sin\nu - R_\mu R_\nu\sin\mu\sin\nu \tag{40}$$

$$\frac{\mathrm{d}z}{\mathrm{d}\mu} = \frac{\mathrm{d}R_\mu}{\mathrm{d}\mu}\sin\mu + R_\mu\cos\mu \tag{41}$$

and

$$\frac{\partial r}{\partial\nu} = \frac{1}{r}\left(x\frac{\partial x}{\partial\nu} + y\frac{\partial y}{\partial\nu}\right) \tag{42}$$

$$\gamma = \tan^{-1}\left(\frac{\partial\theta}{\partial\nu}\right) \tag{43}$$

with

$$\frac{\partial x}{\partial\nu} = R_\mu\frac{\mathrm{d}R_\nu}{\mathrm{d}\nu}\cos\mu\cos\nu - R_\mu R_\nu\cos\mu\sin\nu \tag{44}$$

$$\frac{\partial y}{\partial\nu} = R_\mu\frac{\mathrm{d}R_\nu}{\mathrm{d}\nu}\cos\mu\sin\nu + R_\mu R_\nu\cos\mu\cos\nu \tag{45}$$

R_μ and R_ν are given by (15) and (16), respectively.